

## MAGNETITE–SILICATE INCLUSIONS IN OLIVINE OF OPHIOLITIC METAGABBROS FROM THE MULHACÉN COMPLEX, BETIC CORDILLERA, SOUTHEASTERN SPAIN

ENCARNACIÓN PUGA<sup>§</sup>

*Instituto Andaluz de Ciencias de la Tierra, CSIC, Avda. Fuentenueva, E-18002 Granada, Spain*

MARÍA DOLORES RUIZ CRUZ

*Departamento de Química Inorgánica, Cristalografía y Mineralogía, Facultad de Ciencias, Campus de Teatinos, E-29071 Málaga, Spain*

ANTONIO DÍAZ DE FEDERICO

*Departamento de Mineralogía y Petrología, Facultad de Ciencias, Avda. Fuentenueva, E-18002 Granada, Spain*

### ABSTRACT

Submicroscopic magnetite–silicate inclusions in igneous olivine in metagabbroic rocks from the Betic Ophiolitic Association (BOA) of the Mulhacén Complex, Betic Cordillera, southeastern Spain, have been studied by TEM–AEM. The metamorphic history of these rocks includes a stage of ocean-floor metamorphism followed by polyphase Alpine metamorphism, its metamorphic climax being developed under conditions of subduction. The grains of olivine have a brown color, interpreted as due to blebs of magnetite that formed during the metasomatic and metamorphic processes superimposed on the igneous crystals. The magnetite precipitates display a fixed orientation relative to the olivine host, and form intergrowths with silicate phases. These include monoclinic amphibole, orthorhombic amphibole and monoclinic pyroxene, the association magnetite – monoclinic amphibole being the most common. Chemically, the exsolved amphiboles are calcic and may be subdivided into two types: actinolite, without Na, and edenite and pargasite, containing Na. The presence in the exsolution-induced blebs of a hydrated silicate phase, together with the existence of saline inclusions in the olivine, point to the ocean-floor stage for the influx of seawater, which contributed to the exsolution process. Petrographic observations and comparison of the chemical composition of the exsolved amphiboles with that of the amphiboles developed during the several metamorphic stages registered in the host gabbros allow us to infer the P–T conditions during the exsolution process. Exsolution probably began during ocean-floor metamorphism, and continued during the prograde stage of the eo-Alpine event, at which time the kelyphitic amphibole-bearing coronas formed in the olivine.

*Keywords:* exsolution, magnetite – amphibole – pyroxene, TEM–AEM analysis, olivine metagabbro, ocean-floor metamorphism, Alpine orogeny, Mulhacén Complex, Betic Cordillera, Spain.

### SOMMAIRE

Nous décrivons, au moyen d'analyses TEM–AEM, des inclusions à magnétite + silicates dans l'olivine primaire de roches métagabbroïques de l'association ophiolitique bétique du complexe de Mulhacén, dans la Cordillère Bétique, au sud-est de l'Espagne. L'évolution métamorphique de ces roches a débuté par un épisode de métamorphisme en milieu marin, suivi d'un épisode de métamorphisme alpin polyphasé, menant à un paroxysme dans un milieu de subduction. Les grains d'olivine ont une couleur brune, que nous attribuons à la présence de micro-inclusions de magnétite formées lors des processus métasomatiques et métamorphiques qui ont affecté l'olivine primaire. Les précipités de magnétite démontrent une orientation bien définie par rapport à l'olivine hôte, et sont en intercroissance avec des silicates. Parmi ceux-ci, on a reconnu amphibole monoclinique, amphibole orthorhombique, et pyroxène monoclinique, l'association magnétite – amphibole monoclinique étant la plus répandue. Les amphiboles dans ces intercroissances sont calciques et d'un de deux types, soit actinolite, sans sodium, soit édenite et pargasite, avec sodium. La présence dans ces micro-inclusions formées par exsolution d'un silicate hydraté et l'existence d'inclusions de saumure dans l'olivine témoignent de l'apport de l'eau de mer lors de l'épisode de métamorphisme en milieu marin, qui favorisa le processus d'exsolution. Les observations pétrographiques et une comparaison de la composition chimique des amphiboles exsolvées avec celle des amphiboles développées au cours des divers épisodes de métamorphisme qu'ont subies ces roches

<sup>§</sup> E-mail address: epuga@goliat.ugr.es

gabbroïques permettent de préciser les conditions P–T au cours du processus d'exsolution. L'exsolution a probablement débuté au cours du métamorphisme du fond océanique et s'est prolongée pendant l'épisode prograde de l'événement éoalpin, responsable de la formation de couronnes d'amphibole kelyphitiques dans l'olivine.

(Traduit par la Rédaction)

**Mots-clés:** exsolution, magnétite – amphibole – pyroxène, analyse TEM–AEM, métagabbro à olivine, métamorphisme du fond océanique, orogénèse alpine, complexe de Mulhacén, Cordillère Bétique, Espagne.

## INTRODUCTION

Spinel–silicate precipitates have been identified in both metamorphic and igneous olivines from the Betic Ophiolitic Association (BOA) of the Mulhacén Complex, located in the Betic Cordillera, southeastern Spain. The metamorphic type is a "spinifex"-textured olivine, present in meta-ultramafic rocks; it contains chromite–talc and chromite–enstatite micro-inclusions, whereas the igneous olivine, present in olivine gabbro cumulates, contains magnetite–amphibole precipitates. Both types of rocks were submitted to a stage of ocean-floor metamorphism followed by polyphase Alpine metamorphism. During the Alpine metamorphic climax, developed under conditions of subduction, the ultramafic rocks, previously serpentinized at the oceanic stage, were transformed into "secondary" harzburgites (Puga *et al.* 1999), whereas the gabbroic cumulates were partly transformed to eclogite (Puga *et al.* 1989a). This Complex offers, as a result, an exceptional opportunity to evaluate the influence of factors such as the chemical composition and origin of the parent olivine, as well as other factors related to the metamorphic evolution of the host rock, on the formation of these precipitates.

The exsolution-induced inclusions in olivine of the BOA ultramafic rocks have been recently described by Ruiz Cruz *et al.* (1999). The submicroscopic inclusions of talc identified in that olivine constitute the only case described so far of hydrated silicate phases associated with spinel.

In this contribution, we present results of an electron-microprobe investigation of the BOA cumulitic gabbros and of a TEM/AEM study of the inclusions contained in the olivine that these rocks contain. We elucidate the chemical composition and structure of the inclusions, the mechanisms of their exsolution, and the physicochemical factors of their formation.

## METHODOLOGY

Polished and carbon-coated thin sections were imaged using back-scattered electrons and analyzed by electron microprobe (EMPA), using a Cameca SX–50 instrument. Wollastonite (Si and Ca), synthetic  $\text{Al}_2\text{O}_3$  (Al), orthoclase (K), albite (Na), synthetic  $\text{Fe}_2\text{O}_3$  (Fe), periclase (Mg), and synthetic  $\text{MnTiO}_3$  (Mn and Ti) were used as standards.

From the optical study, a set of olivine grains showing various orientations was selected for the TEM study.

Samples were prepared from thin sections in which grids were attached to the selected areas and later lifted from the glass backing. These areas were ion-thinned and carbon-coated and examined in a 200 kV Philips CM–20 transmission electron microscope (TEM) fitted with a scanning transmission device and a solid-state detector for energy-dispersion analysis (EDX). Micro-analyses were carried out in STEM mode. Quantitative determinations used the thin-film approximation of Cliff & Lorimer (1975). Albite (Na), muscovite and annite (K), albite, spessartine and muscovite (Al), forsterite and annite (Mg and Fe), spessartine (Mn), and titanite (Ca and Ti) were used as standards. Interpolation between Mn and Ti values was used for quantification of Cr concentrations.

The abbreviations of minerals suggested by Kretz (1983) have been used in the text, tables and figures, with some additions indicated in the captions of some figures.

## PETROGRAPHY OF THE SAMPLES

The metabasic rocks of the Mulhacén Complex have been interpreted as being the remains of a dismembered and metamorphosed ophiolitic association (Puga 1990). They are similar to the Western Mediterranean ophiolites of the Ligurian Tethys, and to the rocks dredged from the Atlantic Ridge at 36°N, 45°N and 63°N, *i.e.*, at points with P-type ridge magmatism (Puga *et al.* 1989a, b, 1995). In most cases, the igneous textures and mineral associations have been almost completely obliterated by the metamorphic events. Nevertheless, in the Cóbдар outcrop (Almería Province, southeastern Spain), the primary textures, structures and mineral associations are generally exceptionally well preserved (Puga *et al.* 1989a).

The Cóbдар Formation consists of volcanic, hypabyssal, and plutonic ophiolitic metabasic rocks, dated from the Triassic–Jurassic transition to the Upper Jurassic (Portugal *et al.* 1988, Puga *et al.* 1991, 1995), covered by oceanic metasedimentary rocks containing relics of foraminifera, probably Cretaceous in age (Tendero *et al.* 1993). The base of the Cóbдар Formation is composed of amphibolitized gabbros, and its lowermost limit is a thrust surface with mylonitic rocks and breccias. Above the gabbros, metabasaltic rocks preserve more-or-less deformed pillow-lavas and flow structures, and are cut by sparse basaltic dykes. The plutonic sequence is normally composed of an alternation

of troctolitic cumulates, olivine-pyroxene gabbros, and pyroxene gabbros, mainly transformed to amphibolites, which locally contain relics of an eclogite paragenesis. All these horizons are cut by decimetric to metric metadolerite dykes.

The Córdar metabasic rocks have undergone a complicated metamorphic history, beginning with ocean-floor conditions, followed by the Alpine orogenic conditions, which led to a succession of metamorphic parageneses that, however, only locally obliterated the previous ones (Puga *et al.* 1989a). The process of ocean-floor metamorphism produced mineral associations in the amphibolite and greenschist facies. Subsequently, these metabasic rocks were transformed first to eclogites during an eo-Alpine metamorphic event, and then to albite-epidote amphibolites during a later meso-Alpine event. The most common metamorphic association corresponds to the albite-epidote amphibolite facies; it partly replaces the eo-Alpine eclogite assemblage, or the igneous mineral relics directly.

Figure 1 shows a cumulitic olivine metagabbro in which relics of the igneous texture and paragenesis are preserved. The igneous paragenesis is composed of calcic plagioclase + forsterite + augite + ore minerals, ac-

companied by minor quantities of intercumulus brown amphibole and biotite. The grains of olivine have a brown color due to magnetite precipitates developed during the metasomatic and metamorphic processes superimposed on the igneous crystallization stage. The composition of the more significant primary minerals is reported in Table 1.

The most characteristic mineral formed during the ocean-floor metamorphism is a brown amphibole, which mainly fills millimetric veins in metabasalts, and also appears as isolated crystals along tiny fissures in the matrix of the metagabbro and in the olivine phenocrysts that it contains. This type of amphibole (not visible in Fig. 1) has been dated by the  $^{40}\text{Ar}/^{39}\text{Ar}$  method as upper Jurassic (Puga *et al.* 1991, 1995).

The eo-Alpine stage of metamorphism mainly leads to the development in the gabbros of coronas around the olivine grains in contact with plagioclase (Fig. 1A). In these coronas, the following temporal sequence of blastesis may be deduced from the textural relationships: (1) crystallization of kelyphitic amphibole, (2) replacement of olivine by acicular orthopyroxene, and (3) replacement of the kelyphitic amphibole by almandine and of the acicular orthopyroxene by omphacite. Representative results of chemical analyses of the various metamorphic minerals in the Córdar metagabbros are shown in Table 2.

TABLE 1. SELECTED RESULTS OF EPMA ANALYSES OF IGNEOUS MINERALS IN THE CÓBDAR CUMULITIC GABBRO

	1 Pl core FAC- 1/13	2 Pl rim FAC- 1/12	3 Ol core GCB- 1/1	4 Ol rim GCB- 1/2	5 Cpx PEC- 99/3	6 Amp GCB- 2/49	7 Bt FAC- 1
SiO <sub>2</sub> wt%	53.40	56.30	39.24	39.27	48.81	42.73	35.05
TiO <sub>2</sub>	0.00	0.00	0.01	0.01	2.31	4.37	1.91
Al <sub>2</sub> O <sub>3</sub>	28.78	27.25	0.02	0.02	4.37	11.04	21.17
Cr <sub>2</sub> O <sub>3</sub>	0.00	0.00	0.02	0.02	0.16	0.00	0.01
FeO	0.42	0.39					
FeO			16.81	17.90	7.11	8.64	13.71
MnO	0.00	0.00	0.27	0.27	0.17	0.07	0.05
NiO	0.00	0.00	0.17	0.17	0.02	0.02	0.00
MgO	0.00	0.00	43.35	42.70	14.21	14.93	11.96
CaO	12.00	9.90	0.28	0.24	21.14	11.70	0.04
Na <sub>2</sub> O	4.62	5.76	0.02	0.00	0.56	3.07	0.49
K <sub>2</sub> O	0.20	0.20	0.00	0.00	0.01	0.74	8.94
Total	99.42	99.80	100.20	100.61	98.87	97.30	93.33
Oxygen atoms	8	8	4	4	6	23	22
Si <i>apfu</i>	2.43	2.54	0.99	0.99	1.83	6.38	5.28
<sup>IV</sup> Al	1.55	1.45	0.00	0.00	0.17	1.62	2.72
<sup>VI</sup> Al					0.02	0.33	1.04
Ti	0.00	0.00	0.00	0.00	0.06	0.49	0.22
Cr	0.00	0.00	0.00	0.00	0.00	0.00	0.00
Fe	0.00	0.00	0.36	0.38	0.22	1.08	1.73
Mn	0.00	0.00	0.01	0.01	0.01	0.01	0.01
Ni	0.00	0.00	0.00	0.00	0.00	0.00	0.00
Mg	0.00	0.00	1.64	1.61	0.79	3.33	2.69
Ca	0.59	0.48	0.01	0.01	0.85	1.87	0.01
Na	0.41	0.50	0.00	0.00	0.04	0.89	0.14
K	0.01	0.01	0.00	0.00	0.00	0.14	1.72

Columns: 1: Labradorite, 2: Andesine, 3 and 4: Forsterite, 5: Diopside, 6: Pargasite, 7: Phlogopite. The proportion of cations is expressed in atoms per formula unit (*apfu*).

TABLE 2. SELECTED RESULTS OF EPMA ANALYSES OF METAMORPHIC MINERALS IN THE CÓBDAR CUMULITIC GABBRO

	1 Amp PEC- 99/7	2 Amp FAC- 37/30	3 Opx FAC- 37/35	4 Grt FAC- 37/31	5 Cpx PEC- 99/9	6 Amp PEC- 114/14
SiO <sub>2</sub> wt%	44.07	40.53	53.36	38.95	43.55	43.92
TiO <sub>2</sub>	2.34	0.06	0.01	0.02	0.15	0.12
Al <sub>2</sub> O <sub>3</sub>	10.08	22.68	1.71	21.75	21.79	16.07
FeO	13.84	9.64	17.56	25.00	10.64	15.72
MnO	0.22	0.12	0.58	2.56	0.24	0.21
NiO	0.03	0.00	0.00	0.00	0.02	0.03
MgO	12.47	10.30	25.03	8.83	10.52	7.48
CaO	10.65	9.30	0.91	2.87	7.37	8.22
Na <sub>2</sub> O	2.82	4.55	0.26	0.00	5.36	3.59
K <sub>2</sub> O	0.72	0.18	0.02	0.00	0.33	1.00
Total	97.24	97.37	99.43	99.98	99.96	96.36
Oxygen atoms	23	23	6	12	6	23
Si <i>apfu</i>	6.60	5.83	1.95	3.00	1.54	6.55
<sup>IV</sup> Al	1.40	2.17	0.05	0.00	0.46	1.45
<sup>VI</sup> Al	0.38	1.68	0.03	1.97	0.45	1.38
Ti	0.26	0.01	0.00	0.00	0.00	0.01
Fe	2.00	1.16	0.54	1.61	0.32	1.96
Mn	0.03	0.02	0.02	0.17	0.01	0.03
Ni	0.00	0.00	0.00	0.00	0.00	0.00
Mg	2.78	2.21	1.36	1.01	0.56	1.66
Ca	1.71	1.43	0.04	0.24	0.28	1.31
Na	0.82	1.27	0.02	0.00	0.37	1.04
K	0.14	0.03	0.00	0.00	0.01	0.19

Columns: 1: Edenite of ocean-floor event; 2-5: Pargasite, Enstatite, Almandine and Omphacite of eo-Alpine event; 6: Katophorite of meso-Alpine event. The proportion of cations is expressed in atoms per formula unit (*apfu*).

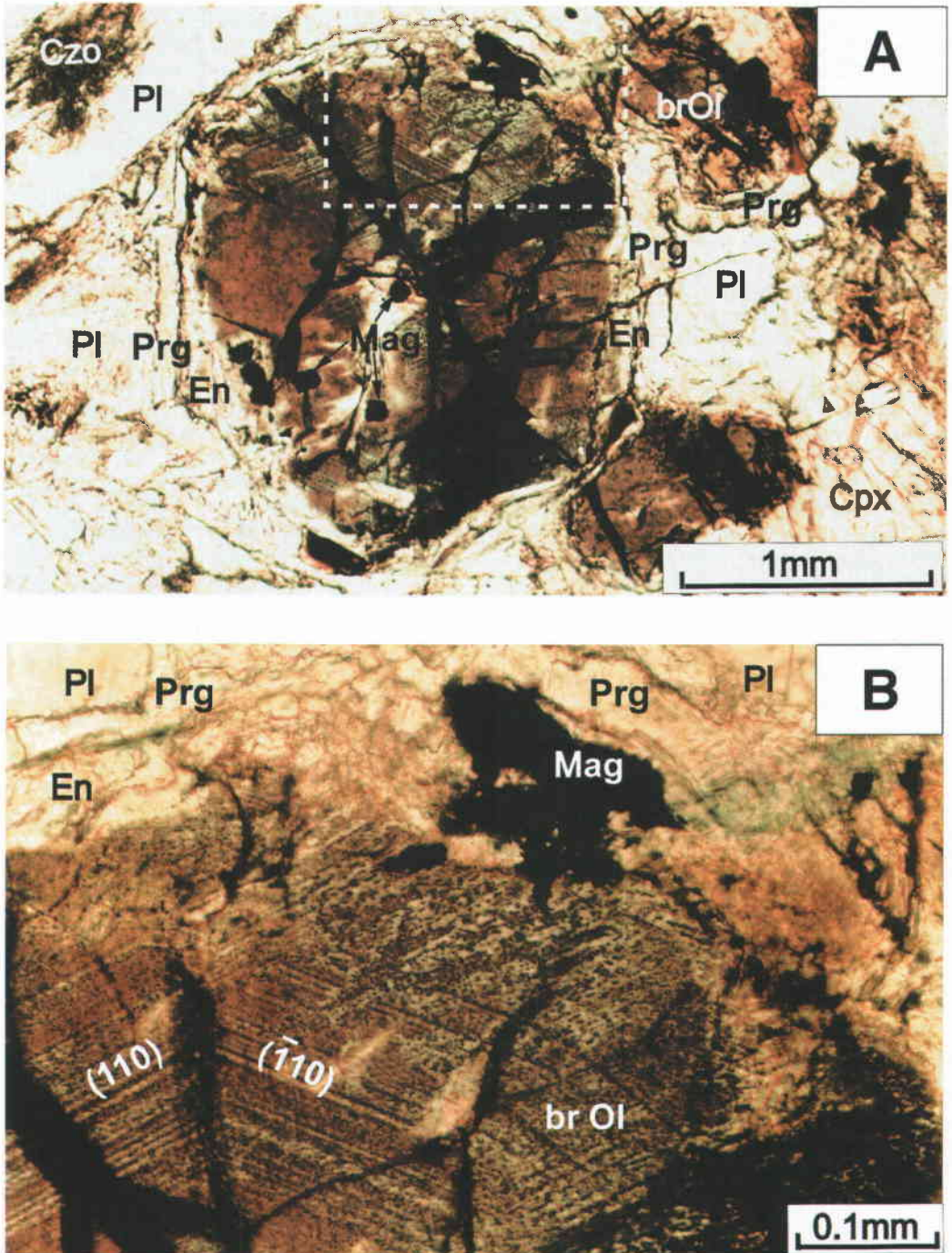


FIG. 1. A. Brown olivine coexisting with primary clinopyroxene (Cpx) and calcic plagioclase (Pl), partly transformed into clinzoisite (Czo) in the core, in a cumulitic olivine metagabbro from the C6bdar region. The olivine contains several microscopic magnetite inclusions (Mag) and is surrounded by a double corona, formed by kelyphitic aggregates of pargasite (Prg), at the rim, and enstatite (En) at the inner zone. B. Enlargement of the white dashed line rectangle, drawn in the upper right part of the brown olivine from A, showing the tiny exsolved crystals of magnetite, concentrated in the (110) and  $(\bar{1}10)$  cleavage planes of the olivine.

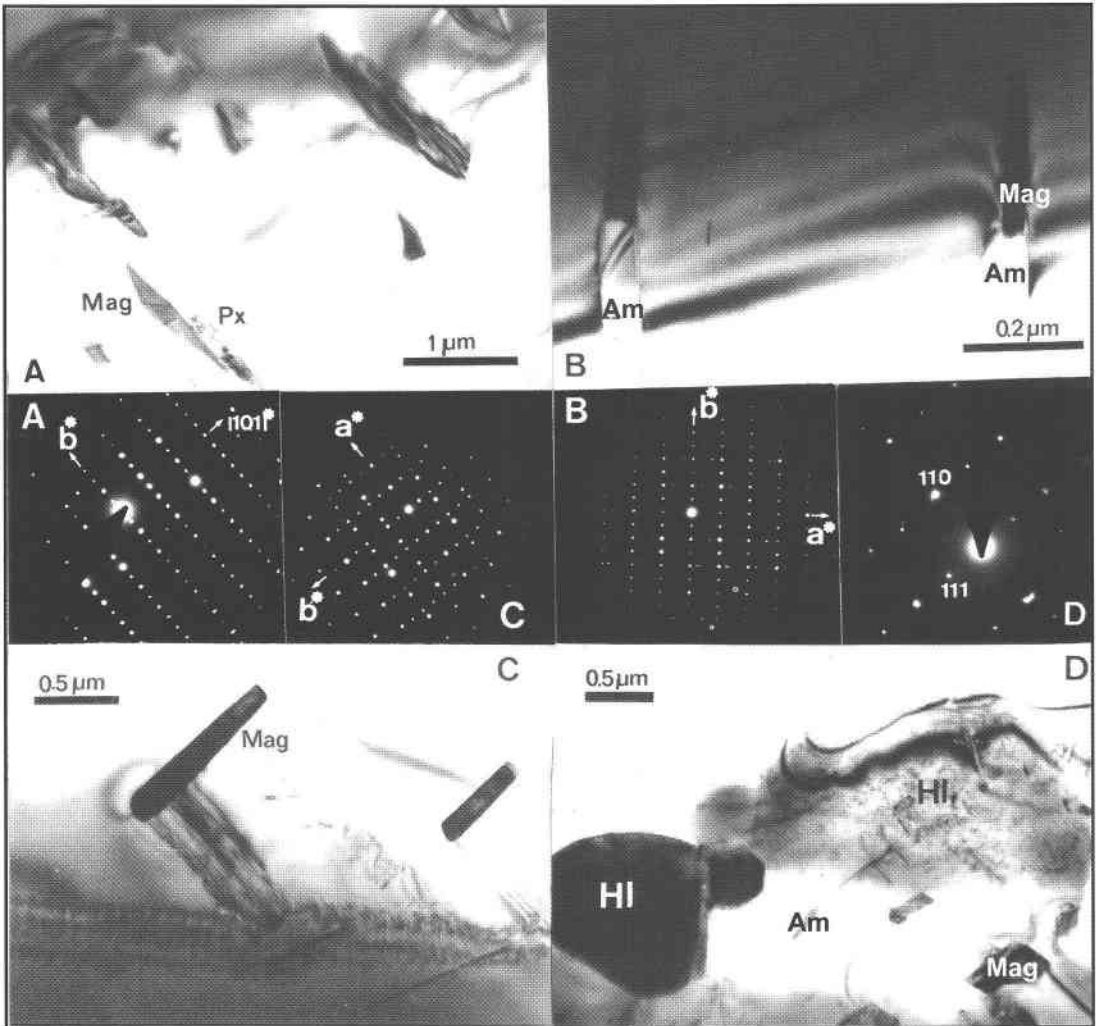


FIG. 2. Low-magnification TEM images showing the most common types of inclusions in olivine. A. Parallel growths of magnetite and pyroxene forming a band perpendicular to (101) of the olivine. The inclusions appear elongate following the *b* axis of the olivine. B. Very elongate inclusions of magnetite–amphibole form bands parallel to the *a* axis of the olivine, whereas the elongation is parallel to the *b* axis of the olivine. C. Oriented inclusions of magnetite formed near the arrays of dislocations. D. Rounded inclusions of NaCl and small magnetite–silicate inclusions. In the SAED patterns A, B and C, which correspond respectively to the textural images A, B and C in this figure, only the directions of olivine have been labeled. The indices in SAED D correspond to NaCl. Am: Amphibole, HI: Halite, Mag: Magnetite, Px: Pyroxene.

#### TEM–AEM RESULTS

Low-magnification TEM observations reveal an irregular, low concentration of precipitates, large areas of the olivine being inclusion-free. The inclusion-bearing and inclusion-free areas may be tentatively correlated with the differently colored bands observed in optical microscopy (Fig. 1B).

Most of the inclusions consist of magnetite and a

silicate phase. The inclusions range in size from 0.1 to 2  $\mu\text{m}$  long, whereas the dimension perpendicular to the elongation is, in most cases, in the order of several hundred  $\text{\AA}$ . Two main types of inclusions occur (Fig. 2). One type shows slightly elongate crystals of magnetite and silicate sharing the longest dimension (Fig. 2A). The other type consists of elongate precipitates in which magnetite and silicate share the shortest dimension of the prisms (Fig. 2B). Complex precipitates showing both



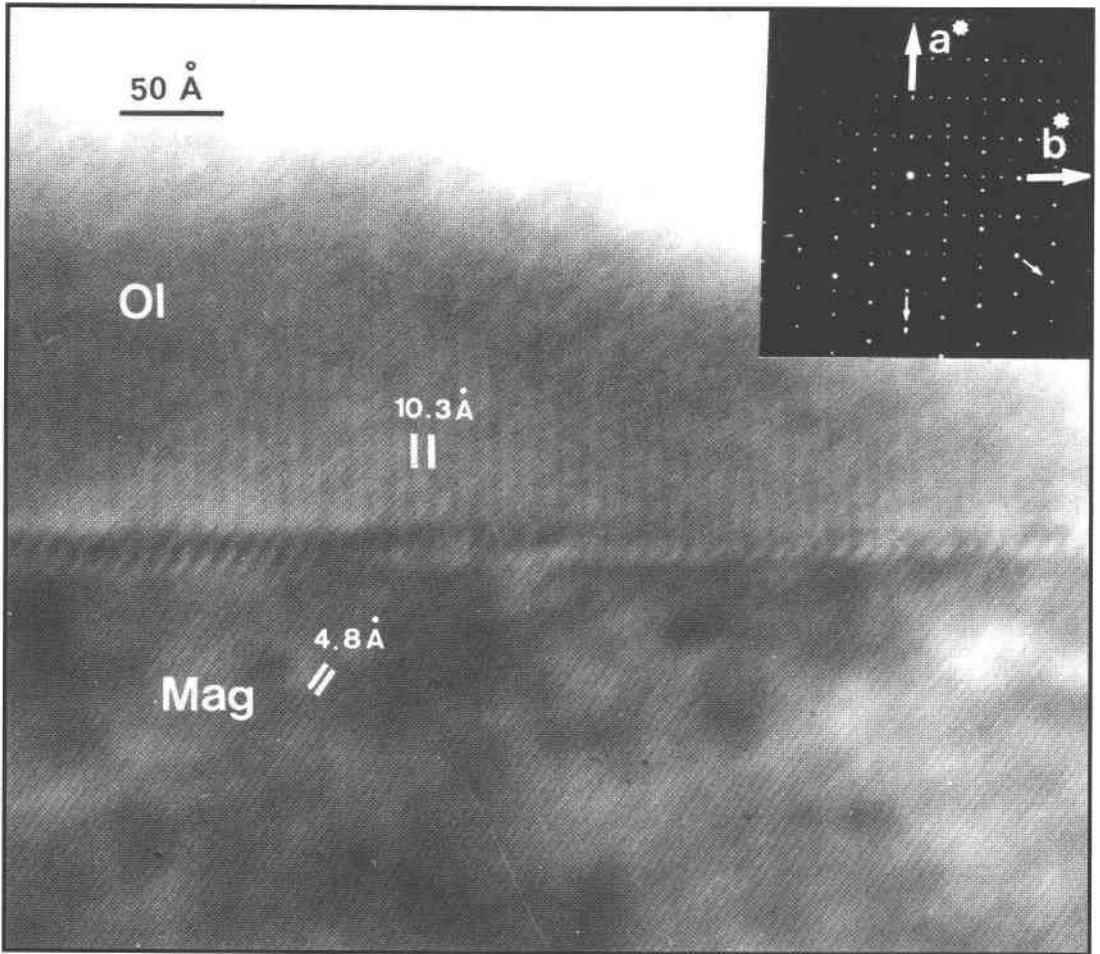


FIG. 3. High-resolution image of the magnetite-olivine boundary. This permits the observation of the fringes with 4.8-Å periodicity corresponding to the (111) planes of the magnetite and the fringes with 10.3-Å periodicity corresponding to the (010) planes of the olivine. The magnetite-olivine boundary shows a narrow zone with moiré fringes, which display a periodicity of about 9.6 Å. The SAED pattern (inset), viewed along the [001] of olivine, shows the orientation relationships between both phases. The large arrows mark the lattice of the olivine, and the small arrows, the [111]\* and equivalent reciprocal directions of the magnetite. Mag: Magnetite; Ol: Olivine.

of olivine and amphibole are parallel, the  $b^*$  axis of the amphibole being parallel to [011] of the olivine. The AEM data of these amphibole inclusions (Table 5) show some contamination by adjacent olivine, as revealed by the ratio  $R = (Si + Al)/(Fe + Mg + Mn + Ca)$ , which should be on the order of 1.1 in actinolitic amphiboles. The most common orientation relationship between olivine and amphibole is shown by the SAED pattern inset in Figure 5, which images the  $a^*-c^*$  plane of the amphibole and the  $a^*-b^*$  plane of the olivine. The lattice-fringe image of the amphibole shows fringes with a 4.5-Å periodicity. These change, in the upper part of the figure, to 18-Å fringes, which are perpendicular to

fringes showing a 10.3-Å periodicity. These may be interpreted as mixed moiré effects due to the superposition of the amphibole and the olivine lattices. Nevertheless, we have also observed periodicities of 9.4 and 10.3 Å, which cannot be explained as moiré fringes, in some other Ca-rich amphibole inclusions, and which suggest the occasional presence of primitive monoclinic lattices. The composition obtained for this inclusion (Table 5) shows minimal contamination, as revealed by the  $R$  value, and the calculated formula (Table 6, anal. 1) corresponds to actinolite.

The Na-bearing calcic amphiboles show structural features different from the Na-free calcic amphiboles.

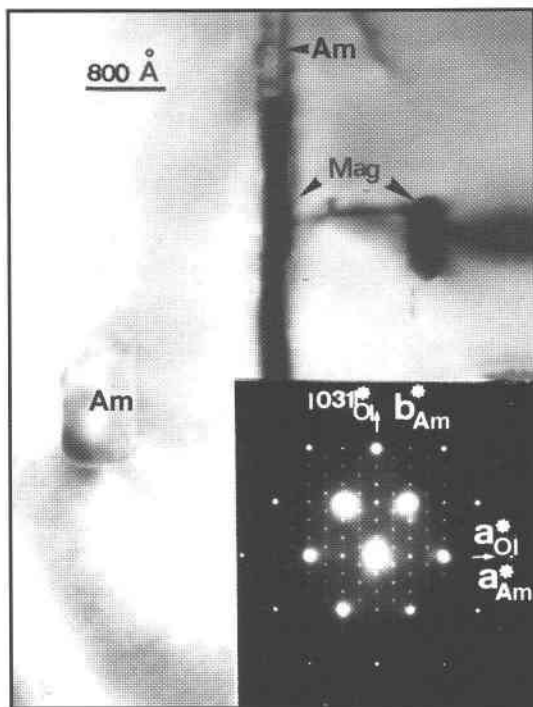


FIG. 4. Single-phase inclusions of amphibole (Am) and magnetite (Mag), and composite amphibole-magnetite inclusion. The SAED pattern (inset) corresponds to the single-phase amphibole inclusion and reveals a  $C$  lattice in which the  $b^*$  axis of the amphibole coincides with the  $[031]^*$  direction of olivine.

Thus Figure 6 shows the TEM images of an amphibole inclusion that displays areas with variable contrast (Fig. 6A). The high-resolution images of the areas with dark contrast display a 4.5-Å periodicity (not shown), whereas the areas with light contrast, which are rapidly damaged, show the transition from 18-Å to 9-Å periodicities along the  $a^*$  axis of the amphibole (Fig. 6B), both showing a 10.3-Å periodicity along  $c^*$ . The SAED pattern A shows reflections of olivine, magnetite and  $C$ -centered monoclinic amphibole. The complex SAED pattern B shows, in addition, weak reflections with about 18-Å periodicity and more intense reflections with about 9-Å periodicity, which correspond to the (100) planes of the amphibole, together with reflections with a 10.3-Å periodicity, which is double that corresponding to the (001) plane of the amphibole. Both directions, being perpendicular, indicate the presence of orthorhombic lattices with a (001) spacing of 10.3 Å. Since this inclusion is relatively large, some analyses free of the contribution from the host phase were made (Table 5), the corresponding structural formulae being shown in Table 6 (anal. 2, 5 and 6).

These analyses reveal a relatively high Al content and variable Na-content, the orthorhombic areas being characterized by higher Na content than the monoclinic ones. Using the nomenclature of the monoclinic amphiboles (Leake *et al.* 1997), these may be classified as edenite and pargasite.

TABLE 5. AEM DATA ON AMPHIBOLE AND PYROXENE INCLUSIONS

	Fig.2A Px	Fig.2B Amp	Fig.4 Amp	Fig.5* Amp	n.s.* Amp	Fig.6 Amp*	Fig.6 Amp*	Fig.6 Amp*
Si atomic %	38.69	39.87	38.82	39.38	51.97	52.71	42.21	39.06
Al	--	0.98	1.90	1.59	2.81	0.91	9.68	11.39
Fe	10.50	7.98	10.97	9.04	8.16	7.44	5.47	5.47
Mg	39.94	44.67	37.49	39.31	24.52	30.82	25.97	23.50
Mn	--	--	--	--	--	--	--	--
Ca	10.87	6.50	10.82	10.68	12.54	13.79	8.12	13.28
Na	--	--	--	--	2.88	7.33	--	3.28
R	0.63	0.69	0.69	0.69	1.21	1.08	1.01	1.15

	Fig.7 Amp	Fig.8* Amp	Fig.9 Px*	Fig.9 Amp	n.s. Px	n.s. Amp	Fig.10A Px	Fig.10A Px	Fig.10B Px*
Si atomic %	38.59	51.20	47.49	39.70	42.94	37.68	37.99	40.46	48.47
Al	1.14	--	1.69	0.60	1.18	1.04	--	--	0.88
Fe	10.19	5.95	3.89	7.20	6.01	11.19	12.95	11.72	6.38
Mg	39.28	30.08	24.27	43.71	30.74	40.67	35.01	34.06	29.79
Mn	--	--	--	--	--	0.24	--	--	--
Ca	10.80	12.77	22.64	8.79	19.05	9.18	14.05	13.76	14.48
Na	--	--	--	--	--	--	--	--	--
R	0.66	1.05	0.97	0.66	0.77	0.63	0.61	0.68	1.00

\* These compositions have been used in Table 6. R = (Si + Al)/(Fe + Mg + Mn + Ca + Na); Amp: Amphibole; Px: Pyroxene; n.s.: compositions of inclusions not shown in the figures.

TABLE 6. STRUCTURAL FORMULAE OF WELL-CHARACTERIZED INCLUDED PHASES

	Amphiboles				Pyroxenes			
	1	Monoclinic phases		4	Orth. phases		Monoclinic	
		2	3		5	6	7	8
Si <i>apfu</i>	7.80	6.34	7.78	7.71	6.66	6.37	7.69	7.65
<sup>IV</sup> Al	0.20	1.66	--	0.13	1.34	1.63	0.26	0.14
<sup>VI</sup> Al	0.22	0.34	--	--	0.18	0.23	--	--
Fe	1.22	1.20	0.90	1.19	0.86	0.89	0.63	1.01
Mg	3.68	4.10	4.58	4.51	4.10	3.83	3.93	4.71
Ca	1.88	1.66	1.94	1.18	2.18	2.16	3.67	2.28
Na	--	0.52	--	--	0.46	1.19	--	--
O	23	23	23	23	23	23	24	24

Structural data and classification: 1.  $C2/m$ : actinolite; 2.  $C2/m$ : edenite; 3. probable monoclinic  $P$  lattice (composition similar to actinolite); 4. probable monoclinic  $P$  lattice (composition intermediate between cummingtonite and actinolite); 5. orthorhombic  $P$  lattice with  $a \approx 9.4$  Å and  $c \approx 10.3$  Å (composition similar to that of magnesian pargasite); 6. orthorhombic  $P$  lattice with  $a \approx 18.2$  Å and  $c \approx 10.3$  Å (composition similar to that of magnesian pargasite); 7.  $C2/c$ : diopside; 8. probable  $P2_1/c$  (composition similar to that of augite). The atomic proportions are quoted in atoms per formula unit (*apfu*).

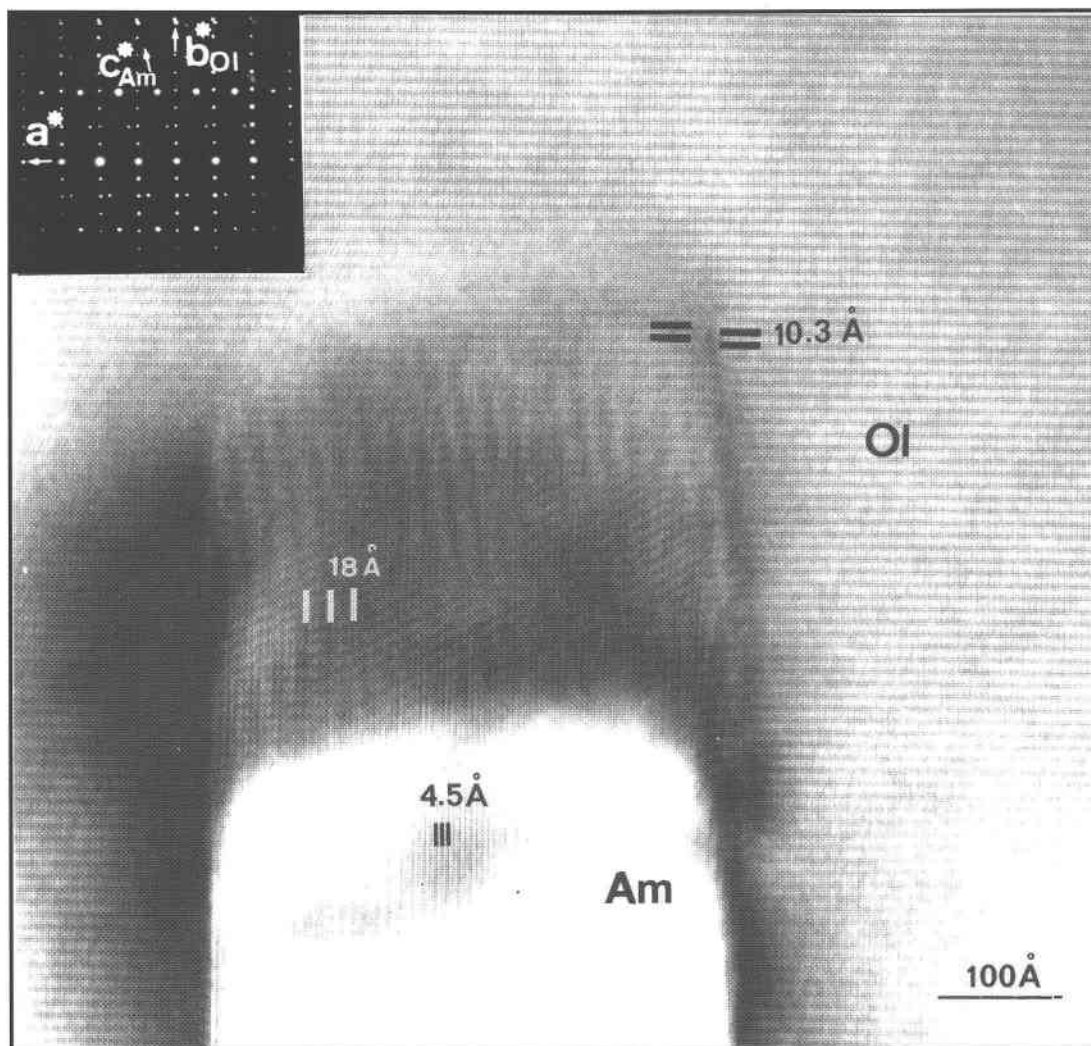


FIG. 5. High-resolution image showing the 4.5-Å periodicity of an amphibole inclusion (Am) and the mixed moiré fringes with 18-Å periodicity, at the boundary amphibole–olivine (Ol). Parallel black lines mark the lack of coincidence between the 10.3-Å fringes of olivine and the 10.3-Å fringes observed in the inclusion. The SAED pattern (inset) shows amphibole reflections corresponding to a *C* lattice.

#### *Composite amphibole – pyroxene – magnetite inclusions*

Two morphological types of composite amphibole – pyroxene – magnetite inclusions have been identified. The first type corresponds to the elongate inclusions, whereas the second corresponds to the shorter inclusions. Transitions between these types also are observed.

In the first case, the amphibole is the dominant silicate phase, whereas the pyroxene forms a thin area that overgrows both amphibole and magnetite (Figs. 7, 8).

The high-resolution image shown in Figure 7 is viewed along  $[0\bar{1}2]$  of olivine, which permits the observation of the  $(110)$  fringes of the amphibole, with a periodicity of about 8.4 Å. The orientation of the  $hh0$  reflection rows of the amphibole, present in the SAED pattern (A), reveals a limited crystallographic control by the olivine structure, the  $a^*$  direction of the olivine being parallel to the  $[31\bar{1}]^*$  of the amphibole. This pattern corresponds to a *C*-centered monoclinic lattice. The high-resolution image reveals the occurrence of a narrow band with fringes having a 9.5-Å periodicity; these overgrow both

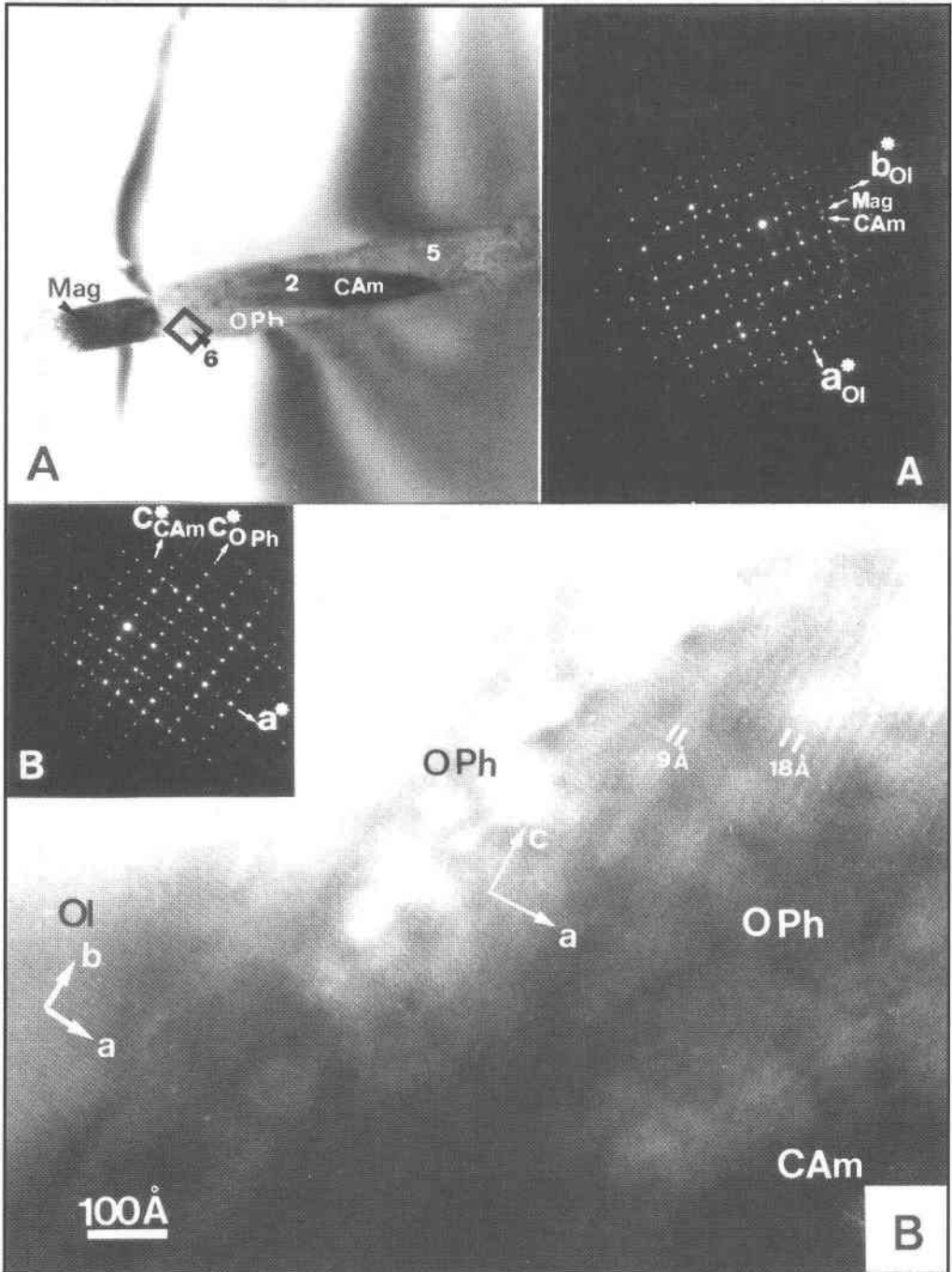


FIG. 6. A. Low-magnification TEM image showing a large magnetite–amphibole inclusion where a monoclinic lamella appears between areas with orthorhombic lattices. SAED pattern A shows reflections of magnetite (Mag) and monoclinic amphibole (CAM). B. Enlargement of the black square drawn on Figure 6A. The high-resolution image reveals that the transition between olivine (Ol) and the 18-Å phase occurs through a narrow area with a periodicity of about 9 Å. The SAED pattern B shows reflections of both clin amphibole (CAM) and orthorhombic phase (OPh), which display a (001) spacing of 10.3 Å. Numbers correspond to compositions shown in Table 6.

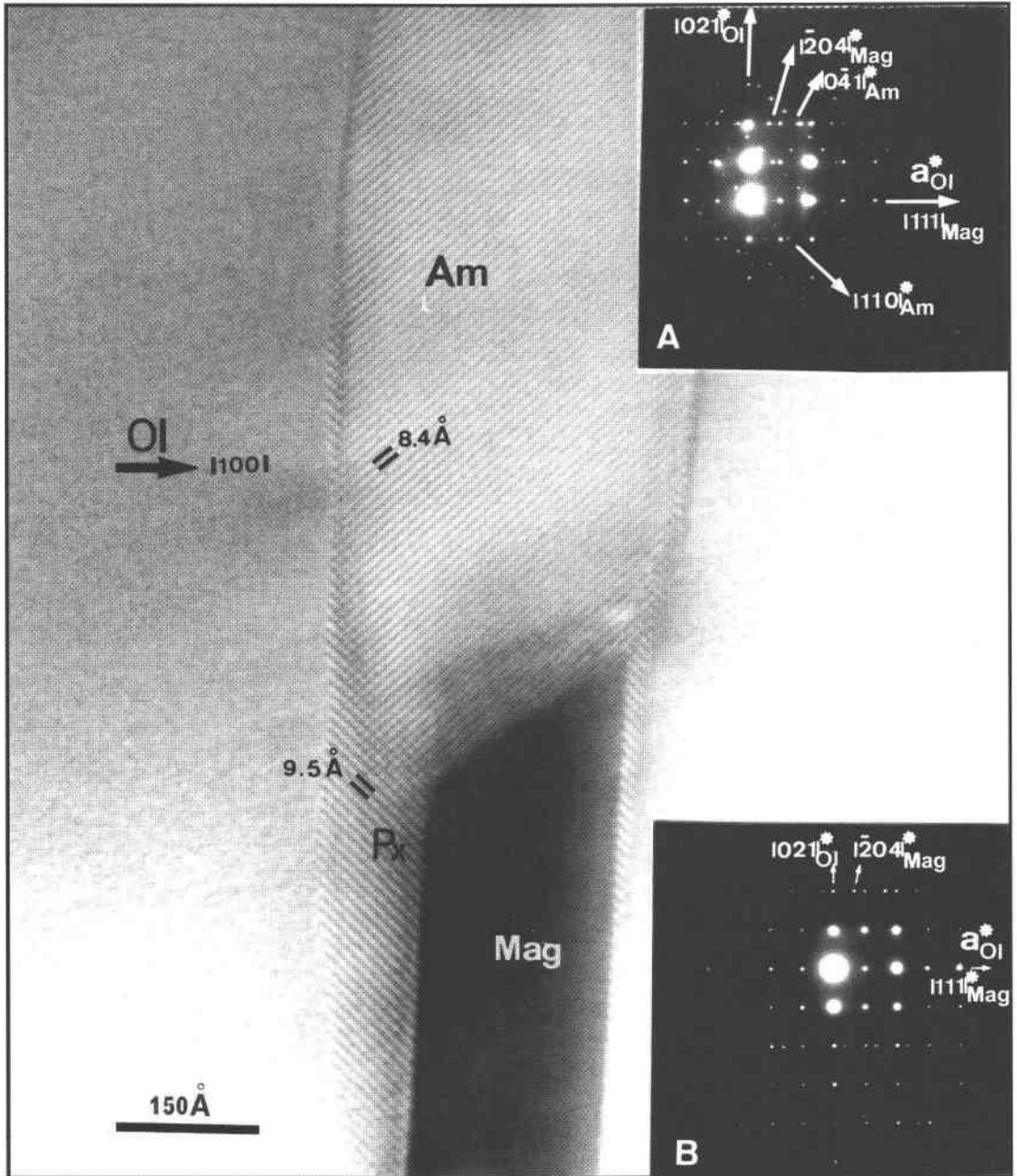


FIG. 7. Lattice-fringe image of a magnetite–amphibole inclusion overgrown by a narrow band of a phase with  $9.5\text{-\AA}$  periodicity, interpreted as pyroxene (*P* lattice). SAED pattern A reveals the poor relationship between amphibole and the host olivine. SAED pattern B shows the orientation relationships between olivine and magnetite. Am: Amphibole, Mag: Magnetite, Ol: olivine, Px: Pyroxene.

the amphibole and the magnetite precipitates. The reflections giving rise to these fringes do not appear in the SAED pattern, but they may be interpreted as corresponding to the (100) planes of pyroxene, on the basis of information obtained in other similar inclusions.

Figure 8 shows a different relative orientation of olivine and amphibole, which permits the observation of the (100) and (010) planes of the olivine but does not allow high-resolution images of the amphibole. Nevertheless, fringes showing a periodicity of about 9 Å also seem to

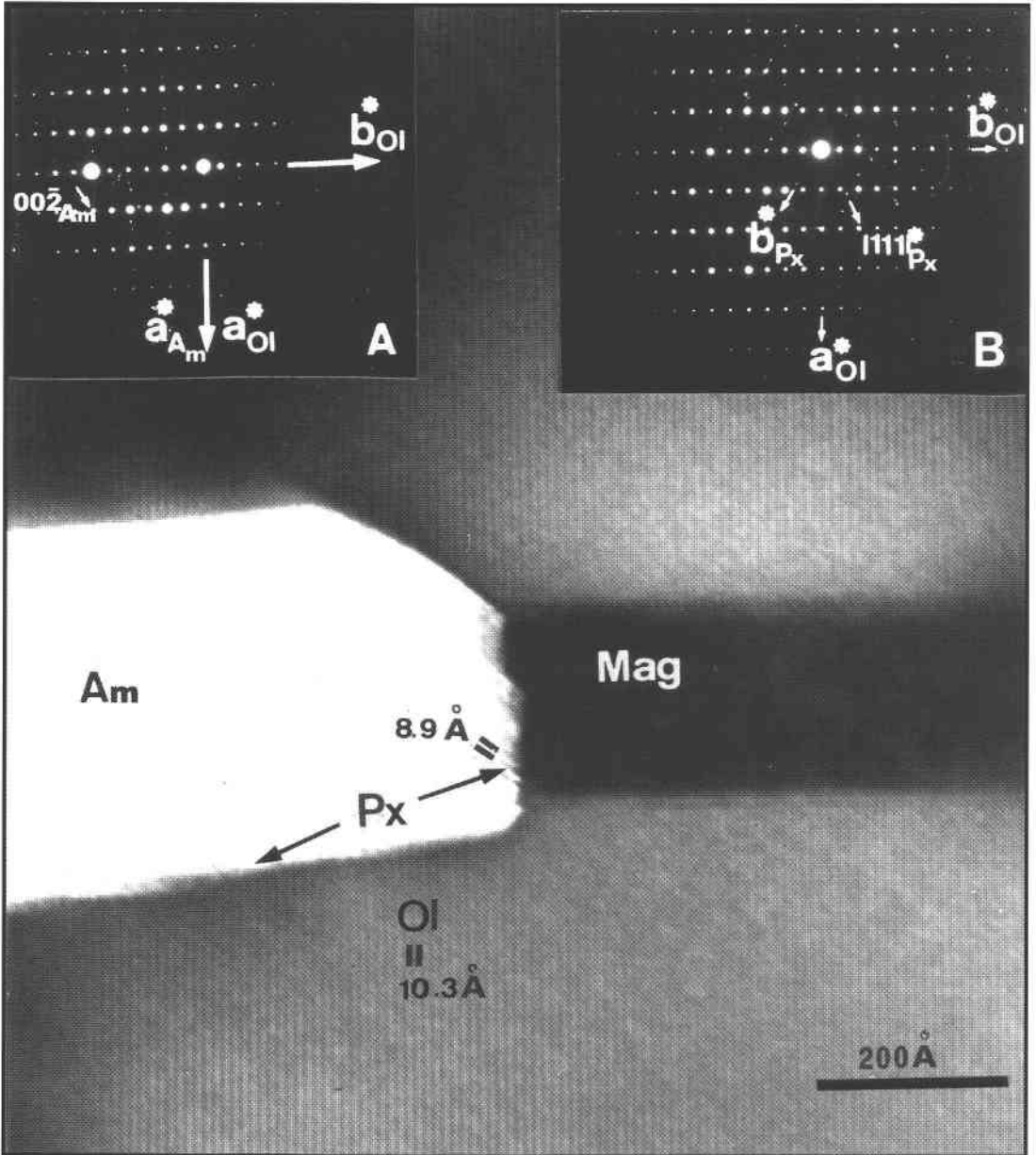


FIG. 8. High-resolution image of a magnetite-amphibole inclusion overgrown by a phase showing 8.9-Å periodicity. This periodicity corresponds, according to the SAED pattern B, to the (010) spacing of pyroxene and reveals a *P* lattice. SAED pattern A shows sparse reflections of an amphibole that shows a 9-Å periodicity along the *a*\* axis, which also indicates a *P* lattice. Am: Amphibole, Mag: Magnetite, Ol: olivine, Px: Pyroxene.

overgrow the amphibole. These fringes belong to a pyroxene, as revealed by the SAED pattern obtained near the interface amphibole–magnetite (B), which indicates a *P* lattice. The SAED pattern obtained from the amphibole precipitate (A) shows weak reflections due to an amphibole, together with intense *hk0* reflections of the host olivine. The periodicity of about 9 Å along the  $a^*$  axis of the amphibole also indicates a *P* lattice. The AEM data for these inclusions (Table 5, anal. 3 in Table 6) are similar to those shown by the amphiboles with a *C*-centered monoclinic lattice. Moseley (1984) attributed the larger parameters of the external phase to an orthopyroxene in a similar overgrowth.

One example of the second morphological type of amphibole – pyroxene – magnetite inclusions is illustrated in Figure 9. The textural relationships between magnetite and amphibole are similar to those described in the amphibole–magnetite inclusions, whereas the shorter precipitates of pyroxene share the longest dimension with magnetite. Figure 9 shows two SAED patterns obtained with different orientations. The SAED pattern

A shows reflections of the type *hk0* of the pyroxene with  $h + k = 2n$ , which indicates a *C*-centered lattice. The SAED pattern B reveals that the orientation relationships between pyroxene and olivine are similar to those determined in pyroxenes overgrowing amphibole (Figs. 7, 8). The AEM data for some of these inclusions (Table 5, anal. 7 in Table 6) reveal that the pyroxene shows a higher Ca content than the associated amphibole. The formulae, calculated from the uncontaminated composition, correspond to diopside.

#### Pyroxene-bearing inclusions

Some rare inclusions show the single association magnetite–pyroxene. Figure 10 shows two of these inclusions. Figure 10A permits the observation of the textural relationships between magnetite and pyroxene, but the corresponding SAED pattern supplies scanty information. In contrast, the SAED pattern obtained with the orientation shown in Figure 10B images the  $b^*-[101]^*$  plane of the pyroxene, which shows a periodicity of 9 Å

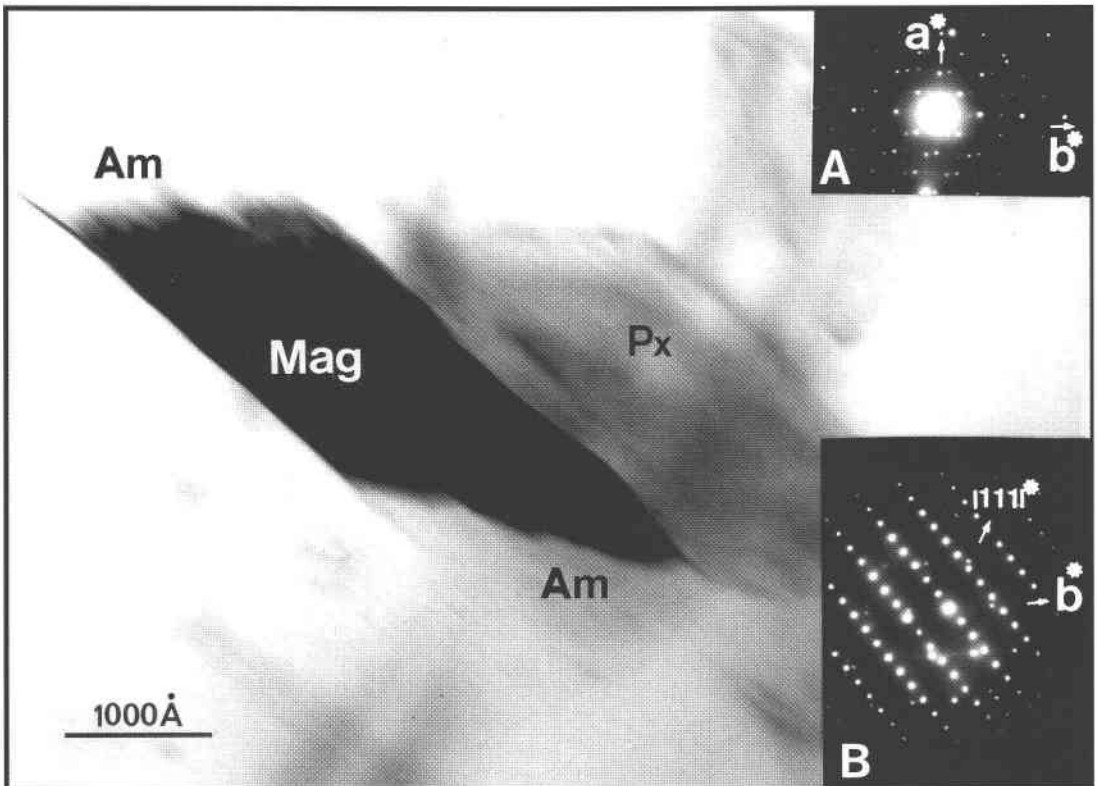


FIG. 9. Magnetite (Mag) – pyroxene (Px) – amphibole (Am) inclusion viewed along the [001] of pyroxene (SAED pattern A). In this pattern, the lack of reflections with  $h + k \neq 2n$  indicates a *C*-centered lattice for pyroxene. The SAED pattern B was obtained with a different orientation, and reveals orientation relationships between olivine and pyroxene similar to those determined in Figure 8. Only the pyroxene directions have been labeled in the SAED patterns.

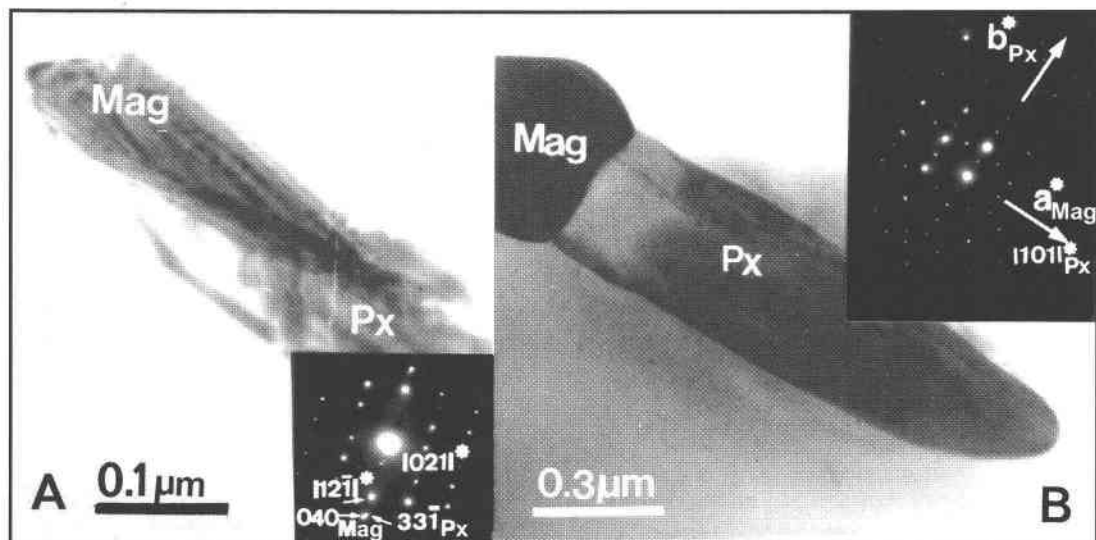


FIG. 10. Low-magnification images of magnetite (Mag) – pyroxene (Px) inclusions, obtained with different orientations. A. This image shows the straight boundary between magnetite and olivine. The SAED pattern (inset) shows intense reflections of olivine and the weaker ones of magnetite (Mag) and pyroxene (Px). B. This image shows the aspect of the magnetite–pyroxene inclusions with a different inclination. The SAED pattern (inset) reveals close orientational relationships between magnetite and pyroxene. The latter shows a (010) spacing of 9 Å, which indicates a *P* monoclinic lattice.

along the  $b^*$  axis, and may be interpreted as belonging to a monoclinic *P* lattice. This pattern also illustrates the orientation relationships between pyroxene and magnetite, the  $a^*$  direction of the magnetite being parallel to the  $[101]^*$  of the pyroxene, which suggests that the orientation of the pyroxene is not controlled by the host olivine but by the structure of magnetite. The AEM data for some of these inclusions (Table 5) permit the deduction of the formula, which corresponds to augite (anal. 8 in Table 6).

#### DISCUSSION

##### *Origin and sequence of crystallization of spinel and silicate precipitates*

The magnetite–silicate precipitates in olivine from gabbro, described here, as well as those of chromite–enstatite and chromite–talc in “spinifex”-textured olivine from the BOA ultramafic rocks (Ruiz Cruz *et al.* 1999), show close similarities in morphology and orientation to some precipitates previously identified in other ultramafic and mafic rock outcrops, which were interpreted as originating by exsolution (*e.g.*, Putnis 1979, Moseley 1984, Banfield *et al.* 1990). Nevertheless, the presence of hydrated phases (amphibole in the case of the gabbros and talc in the case of the ultramafic rocks of the BOA) is a peculiarity of inclusions in olivine from these meta-ophiolitic rocks. This peculiarity

clearly indicates that availability of  $H_2O$ , probably related with the metamorphic episodes that affected the BOA host rocks, was an important factor controlling both the composition and the structure of the silicate phases formed by exsolution.

Two main hypotheses have been put forward to explain the occurrence of spinel–pyroxene intergrowths in olivine. The first hypothesis, based on observational data, assumes that exsolution occurred by solid-state diffusion and precipitation of phases hosting minor elements, such as Cr, Ti or Ca, out of the olivine structure (Bell *et al.* 1975, Arai 1978, Moseley 1984). The second hypothesis, based on experimental data (Champness & Gay 1968, Champness 1970), assumes that exsolution of spinel and pyroxene follows the oxidation of the olivine (Goode 1974, Kohlstedt & Vander Sande 1975, Putnis 1979, Banfield *et al.* 1990).

In the inclusions studied here, the oxidation of olivine, which would result in the direct formation of magnetite, seems to be the most likely initial mechanism. In fact, the concentration of inclusions in olivine is not homogeneous; the inclusions-rich areas, as revealed by the brown color, preferentially develop near the margins of the grains and following microfissures (Fig. 1), zones in which the oxidation would be expected to occur preferentially (Banfield *et al.* 1990). Moreover, the presence of a magnetite core in some of the silicate inclusions (*e.g.*, Fig. 9) suggests that magnetite may locally be the first phase to precipitate. The development

of silicate precipitates would follow, owing to solid-state diffusion, as a host for minor elements such as Ca, previously located in the olivine structure, and, more locally, Na, which probably derives from saline inclusions contained in it.

The almost simultaneous precipitation of amphibole and magnetite and the subsequent precipitation of pyroxene probably determined the orientational relationships among the different phases, some of which had not been previously described. The orientation of magnetite is clearly controlled by the structure of the host olivine, the planes of close-packed oxygen atoms being parallel in both structures. This orientation, which is typical in exsolved spinel, leads to coherent boundaries between olivine and magnetite. Similarly, the orientation of the amphibole precipitates relative to the olivine maintains, in most of the precipitates, the (100) planes of the olivine parallel to the (100) planes of the amphibole, also indicating that the amphibole growth was controlled by the host olivine. This orientational relationship favors the rapid growth of the amphibole crystals parallel to the *c* axis, and the slower growth perpendicular to this direction, thus explaining the shape of the magnetite-amphibole inclusions. These relationships between olivine and amphibole also favor the formation of coherent boundaries between these phases, along the longest dimension of the precipitates. The accommodation of the olivine and amphibole structures is, on the contrary, more difficult along the *c* axis of the amphibole, and leads to incoherent boundaries, along which the presence of defects leads to rapid damage in the electron beam.

In contrast to the precipitates of magnetite and amphibole, both the pyroxene inclusions and the pyroxene overgrowths in composite inclusions show subtle orientational relationships with the host olivine. A closer relation is, however, observed between magnetite and pyroxene orientations, indicating that the growth of the pyroxene was mainly controlled by the orientation of the previously formed magnetite. These relations account for the coherent boundaries between magnetite and pyroxene, which share well-developed faces, and incoherent ones between pyroxene and olivine (*e.g.*, Fig. 7).

The orthorhombic structures observed in some amphiboles commonly develop at the amphibole-olivine boundaries (Fig. 6) and may be tentatively interpreted as superstructures, which would favor the accommodation of the olivine and the amphibole lattices. Another question arises from the presence of monoclinic *P* lattices in some of the pyroxene and amphibole precipitates. Commonly, the pyroboles showing such a lattice are Ca-poor (*e.g.*, cummingtonite, pigeonite and kanoite), the transition from the ordered *P* lattice to the disordered *C* lattice being a displacive, temperature-dependent reaction (Ross *et al.* 1968, 1969, Papike *et al.* 1969, Brown *et al.* 1972, Arlt & Armbruster 1997). Nevertheless, Woensdregt & Hartman (1969) identified

hornblende with *P2<sub>1</sub>/m* symmetry. Similarly, the ordered *P2<sub>1</sub>/n* space group has been identified in omphacite (Matsumoto *et al.* 1975), this structure being interpreted as due to the presence of some order of Mg and Al in two different *M1* sites and of Na and Ca in two *M2* sites (Rossi *et al.* 1983, Boffa Ballaran *et al.* 1998). Recently, both *C2/c* and *P2<sub>1</sub>/c* clinopyroxenes were identified during the thermal decomposition of tremolite by Xu *et al.* (1996). The chemical formulae deduced from the AEM analyses indicate in that case that the *P2<sub>1</sub>/c* clinopyroxene is enriched in Mg, whereas the *C2/c* clinopyroxene is enriched in Ca. In the opinion of Xu *et al.*, the decomposition of tremolite was accompanied by a segregation of Ca and Mg atoms. In fact, the compositions we have obtained in both *C2/c* and probable *P2<sub>1</sub>/c* structures show a similar trend, the *C2/c* structure showing higher Ca content and lower (Mg + Fe) content than the primitive structure (anal. 7, 8 in Table 6). In our opinion, the primitive lattices identified in both pyroxene and amphibole inclusions probably represent intermediate, metastable phases, the formation of which would require lower activation energy, because their structure is more closely related to that of the host olivine. A similar interpretation was proposed by Champness & Lorimer (1974) to explain the presence of Ca-enriched primitive pyroxene exsolved in orthopyroxene.

#### *Time and the physical conditions of formation of the precipitates*

Several types of criteria, including textural, chemical, and mineralogical ones, may be used in the interpretation of time and physical conditions of formation of the precipitates.

The textural relationships between the oxidized olivine and the surrounding corona indicate that the oxidation process began before, or concomitantly with, the beginning of corona development, and progressed during this process. This fact would explain how the olivine surrounded by incipient coronas of amphibole (normally less than 0.1 mm in thickness) only show the brown color in the external part of the rim and over irregular patches. On the other hand, the olivine grains that are totally brown in color, showing evidence of a more advanced and homogeneous process of exsolution, are surrounded by thicker amphibole-enstatite double coronas, which completely replace the smaller crystals of olivine (Fig. 1A). A comparison of the physical conditions of development of amphibole in various ocean-floor environments, mainly leading to a corona as a result of the olivine + plagioclase reaction, with the conditions in which the amphibole-bearing coronas surrounding the olivine were formed in the C6bdar gabbros, suggests an orogenic origin for the latter. Moreover, the coronas were formed prior to the eo-Alpine metamorphic climax, during which they were replaced by the almandine + omphacite paragenesis of eclogites. In

other words, exsolution must occur, at least in part, during the prograde eo-Alpine stage. The required oxidizing conditions for the formation of magnetite and the mobility of the fluid phase could have been attained either during the ocean-floor metamorphic stage or during the subsequent metamorphic process under conditions of subduction. Nevertheless, some mineralogical and chemical criteria point to the ocean-floor stage as the most probable for the beginning of the exsolution process or, at least, for the influx of minor amounts of seawater into the olivine, facilitating the local development of both the hydrous silicates as exsolved minerals and the saline inclusions also present in the olivine (Fig. 2D). Seawater penetration in the olivine gabbro during this stage of metamorphism had to have taken place above the stability field of serpentine because this mineral has not been found among the precipitated phases. High-T conditions, near or above 500°C, are common at the gabbroic levels of the oceanic crust near slow-spreading oceanic ridges (Ito & Anderson 1983, Gillis *et al.* 1993), and also during the eo-Alpine stage of prograde metamorphism in the subsequent episode of subduction (Puga *et al.* 1989a, b, 1995; Ruiz Cruz *et al.* 1999).

In an attempt to elucidate more precisely the physical conditions under which exsolution could have taken place, we have compared the chemical composition of the exsolved amphiboles with that of the amphibole coronas surrounding the olivine, and with other types of amphibole present in the metagabbro matrix and in other C6bdar metabasic rocks (Figs. 11, 12). We have also plotted, in these figures, the composition of amphiboles of basic rocks, mainly forming coronas, from various locations on the present ocean floor along the Mid-Atlantic Ridge (MAR) and the Mid-Cayman Rise (MCR); these amphiboles are interpreted as products of ocean-floor metamorphism (Ito & Anderson 1983, Gillis *et al.* 1993). The comparison is constrained by two factors: a) the small size of precipitates, which makes it unlikely to obtain uncontaminated compositions of amphibole, and b) the irregular and difficult entry of fluids in the olivine, to provide the Al, Ca and Na necessary to form the silicate inclusions, as these are not present in the olivine structure.

The better characterized inclusions of amphibole (Table 6) are subdivided into two types, corresponding to Na-free calcic amphibole of actinolite composition and Na-bearing calcic amphiboles of edenite and pargasite composition. All these amphiboles have a lower Al content than the majority of the amphiboles plotted in Figure 11. Some similarities may be envisaged between the  $^{IV}Al$  values in inclusions of the Na-bearing calcic amphibole type and the C6bdar ocean-floor brown amphiboles. The ratio  $^{VI}Al/Al$  (= fAl) is directly dependent on the pressure of amphibole development, according to Smith (1988), whereas the  $^{IV}Al$  value normally increases with temperature, as also do their Ti content and  $^{IV}Al/Al$  values. A plot of fAl *versus*

$^{IV}Al$  in the amphibole inclusions (Fig. 11) suggests a wide range of P for the actinolite inclusions, similar to that corresponding to the field of C6bdar coronas, whereas the Na-bearing calcic amphibole type, with a lower value of fAl, could have been developed at lower-P conditions than the coronas, and even lower than those registered for the amphiboles formed at present ocean-floor locations, and at similar T conditions to those deduced for the C6bdar ocean-floor amphiboles.

Figure 12 allows an estimation of the P conditions for the various types of amphiboles, from C6bdar and the oceanic environments, represented in Figure 11, on the basis of their  $^{23}Na$  *versus*  $^{IV}Al$  values. According to this diagram, proposed by Brown (1977) for amphiboles developed by metamorphism of basic rocks, the C6bdar orogenic coronas were developed in a range from about 2 to 7 kbar, whereas the ocean-floor coronas and the amphiboles from the C6bdar metabasic rocks, interpreted to have formed at conditions of ocean-floor metamorphism (Puga *et al.* 1989a), would have developed below 2 kbar. We have also represented in this figure the composition of the exsolved amphiboles. Their Na content, being very low or nil (Fig. 12, Table 6), makes it impossible to estimate directly the pressure of their formation using Brown's diagram, which is valid for calcic amphibole coexisting with albite, among other phases. The absence of orthopyroxene as precipitates in the C6bdar olivine, despite its presence in the inner coronas surrounding this mineral (Fig. 1a), could reflect the fact that the pressure conditions during the exsolution process were lower than those attained during the development of the inner orthopyroxene-bearing coronas.

#### CONCLUDING REMARKS

Magnetite – amphibole – pyroxene micro-inclusions, present in olivine from the BOA cumulitic gabbros, are interpreted as precipitates formed by high-temperature exsolution, which followed the oxidation of the host olivine. Actinolite, edenite and pargasite were identified among the amphibole inclusions, whereas the composition of the associated pyroxene corresponds to diopside and augite. These silicate precipitates differ from the previously described ones by the presence of a hydrated phase, which indicates that availability of  $H_2O$  was an important factor controlling the type of silicate phase formed during exsolution.

Textural relationships between the oxidized olivine and the surrounding coronas, as well as chemical and mineralogical criteria, point to an early stage of ocean-floor metamorphism as the most probable for both the influx of seawater in olivine, the oxidation of the olivine, and the beginning of the exsolution process, which seems to have continued during the prograde eo-Alpine stage, together with the development of coronas around the olivine. The influx of hydrous fluids in the BOA olivine gabbros during the ocean-floor stage would also

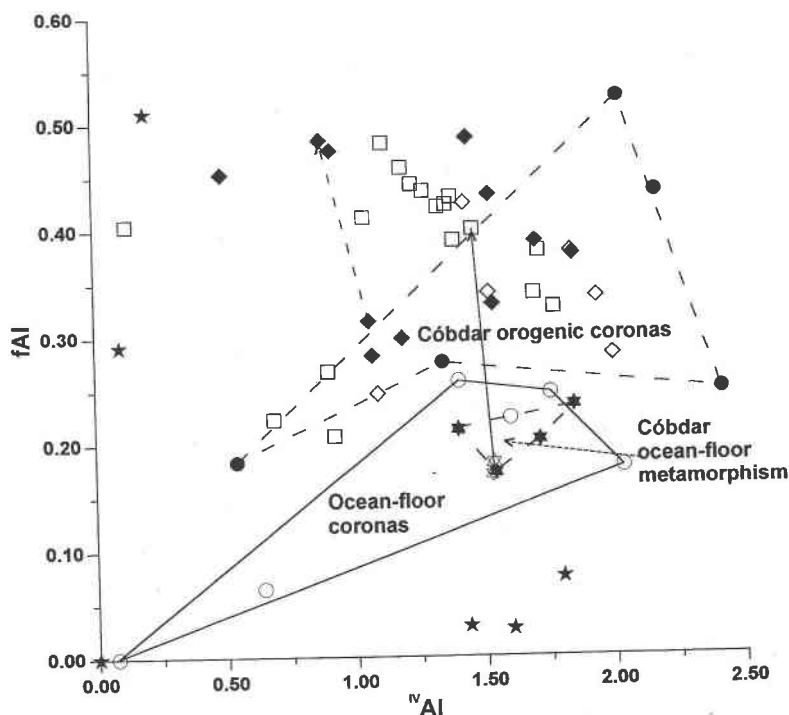


FIG. 11. Plot of  $fAl$  ( $^{VI}Al/Al$ ) versus  $^{IV}Al$  of amphiboles exsolved in olivine of the BOA cumulitic gabbros, compared with other examples of metamorphic amphibole from both the Córdoba metabasic rocks and the olivine gabbros dredged from the MAR and MCR, affected by ocean-floor metamorphism (Ito & Anderson 1983, Gillis *et al.* 1993). Key for symbols corresponding to amphiboles in different microdomains of the BOA cumulitic gabbros: five-pointed stars: exsolution-related amphibole in olivine; full dots: kelyphitic amphibole surrounding olivine; full six-pointed stars: ocean-floor amphiboles formed along fissures in olivine and in the rock matrix; full diamonds: meso-Alpine amphiboles replacing eo-Alpine pyroxene. Symbols for amphiboles from other Córdoba ophiolitic lithotypes: open diamonds: metadolerite, open squares: metabasalt, open six-pointed stars: veins formed by ocean-floor metamorphism in metabasalts. Circles: kelyphitic amphibole-bearing coronas in ocean-floor olivine gabbros from the MAR and MCR. Continuous arrows represent normal evolutionary trends in the Córdoba outcrop, from brown Ti-rich amphiboles to green or blue-green amphiboles with high values of  $fAl$ .

explain the presence of submicroscopic inclusions of NaCl alongside the other precipitate phases in the olivine. Thus, in contrast to most of the previously described cases of exsolution in olivine, in which this process is mainly related either to subsolidus cooling or to oxidation of this mineral during weathering, the complex history of these ophiolitic metagabbros seems to present the physicochemical conditions needed for the formation of exsolved phases in olivine by a high-temperature episode of oxidation during metamorphic recrystallization.

#### ACKNOWLEDGEMENTS

The authors are very grateful to R. Compagnoni and G. Ferraris (Torino), M. Mellini (Siena) and R.F. Mar-

tin (Montreal), whose fruitful critical reviews have notably improved the manuscript. They are also indebted to M.M. Abad for help in obtaining the TEM-AEM data, to J.M. Nieto for his fruitful discussions during the interpretation of the results, and to A. Diaz Puga and A. Molina for the production of the photos. Financial support from Spanish Project PB 95-0220 and from the Research Group of the Junta de Andalucía RMN187 is acknowledged.

#### REFERENCES

- ARAI, S. (1978): Chromian spinel lamellae in olivine from the Iwanai-Dake peridotite mass, Hokkaido, Japan. *Earth Planet. Sci. Lett.* **39**, 267-273.

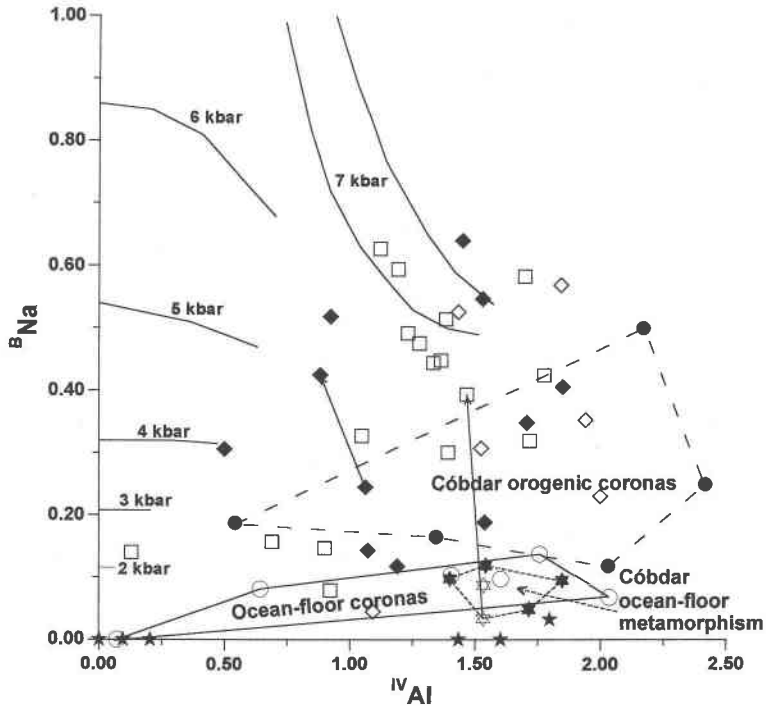


FIG. 12. Plot of  $B_{Na}$  versus  $IV_{Al}$  for the different types of amphibole represented in Figure 11, and with the same symbols. This figure shows a lower-P range of conditions for the Córdoba ocean-floor amphiboles than for those forming eo-Alpine coronas and most of the meso-Alpine amphiboles. Continuous arrows indicate the different pressures estimated for the development of the cores in the brown amphibole of metagabbros (full diamonds) and metabasalts (open six-pointed stars), and their respective overgrowth (rim).

- ARLT, T. & ARMBRUSTER, T. (1997): The temperature-dependent  $P2_1/c-C2/c$  phase transition in the clinopyroxene kanoite  $MnMg[Si_2O_6]$ : a single-crystal X-ray and optical study. *Eur. J. Mineral.* **9**, 953-964.
- BANFIELD, J.F., VEBLEN, D.R. & JONES, B.F. (1990): Transmission electron microscopy of subsolidus oxidation and weathering of olivine. *Contrib. Mineral. Petrol.* **106**, 110-123.
- BELL, P.M., MAO, H.K., ROEDDER, E. & WEIBLEN, P.W. (1975): The problem of the origin of symplectites in olivine-bearing lunar rocks. *Proc. Sixth Lunar Sci. Conf.* **1**, 231-248.
- BOFFA BALLARAN, T., CARPENTER, M.A., DOMENEGHETTI, M.C. & TAZZOLI, V. (1998): Structural mechanisms of solid solution and cation ordering in augite-jadeite pyroxenes. I. A macroscopic perspective. *Am. Mineral.* **83**, 419-433.
- BOLAND, J.N., MCLAREN, A.C. & HOBBS, B.E. (1971): Dislocations associated with optical features in naturally-deformed olivine. *Contrib. Mineral. Petrol.* **30**, 53-63.
- BROWN, E.H. (1977): The crossite content of Ca-amphibole as a guide to pressure of metamorphism. *J. Petrol.* **18**, 53-72.
- BROWN, G.E., PREWITT, C.T., PAPIKE, J.J. & SUENO, S. (1972): A comparison of the structures of low and high pigeonite. *J. Geophys. Res.* **77**, 5778-5789.
- CHAMPNESS, P.E. (1970): Nucleation and growth of iron oxides in olivines,  $(Mg,Fe)_2SiO_4$ . *Mineral. Mag.* **37**, 790-800.
- \_\_\_\_\_ & GAY, P. (1968): Oxidation of olivines. *Nature* **218**, 157-158.
- \_\_\_\_\_ & LORIMER, G.W. (1974): A direct lattice-resolution study of precipitation (exsolution) in orthopyroxene. *Phil. Mag.* **30**, 357-365.
- CLIFF, G. & LORIMER, G.W. (1975): The quantitative analysis of thin specimens. *J. Microscopy* **103**, 203-207.
- GILLIS, K.M., THOMPSON, G. & KELLEY, D.S. (1993): A view of the lower crustal component of hydrothermal systems at the Mid-Atlantic Ridge. *J. Geophys. Res.* **98**, 19,597-19,619.

- GOODE, A.D.T. (1974): Oxidation of natural olivines. *Nature* **248**, 500-501.
- ITO, E. & ANDERSON, A.T., JR. (1983): Submarine metamorphism of Gabbros from the Mid-Cayman Rise: petrographic and mineralogic constraints on hydrothermal processes at slow-spreading ridges. *Contrib. Mineral. Petrol.* **82**, 371-388.
- KOHLSTEDT, D.L. & VANDER SANDE, J.B. (1975): An electron microscopy study of naturally occurring oxidation produced precipitates in iron-bearing olivines. *Contrib. Mineral. Petrol.* **53**, 13-24.
- KRETZ, R. (1983): Symbols for rock-forming minerals. *Am. Mineral.* **68**, 277-279.
- LEAKE, B.E., WOOLLEY, A.R., ARPS, C.E.S., BIRCH, W.D., GILBERT, M.C., GRICE, J.D., HAWTHORNE, F.C., KATO, A., KISCH, H.J., KRIVOVICHEV, V.G., LINTHOUT, K., LAIRD, J., MANDARINO, J.A., MARESCH, W.V., NICKEL, E.H., ROCK, N.M.S., SCHUMACHER, J.C., SMITH, D.C., STEPHENSON, N.C.N., UNGARETTI, L., WHITTAKER, E.J.W. & GUO, YOUZHI (1997): Nomenclature of amphiboles: report of the Subcommittee on Amphiboles of the International Mineralogical Association, Commission on New Minerals and Mineral Names. *Can. Mineral.* **35**, 219-246.
- MATSUMOTO, T., TOKONAMI, M. & MORIMOTO, N. (1975): The crystal structure of omphacite. *Am. Mineral.* **60**, 634-641.
- MOSELEY, D. (1984): Symplectic exsolution in olivine. *Am. Mineral.* **69**, 139-153.
- OTTEN, M.T. (1985): The subsolidus history of the Artfjället gabbro: a TEM study of olivine, augite and orthopyroxene. *J. Petrol.* **26**, 488-514.
- PAPIKE, J.J., ROSS, M. & CLARK, J.R. (1969): Crystal chemical characterization of clin amphiboles based on five new structure refinements. *Mineral. Soc. Am., Spec. Pap.* **2**, 117-136.
- PORTUGAL, M., FERREIRA, J.D., PUGA, E. & DÍAZ DE FEDERICO, A. (1988): Geochronological contribution to the petrogenetic picture of the Betic Chain, SE Spain. *Com. II Congreso Geol. España* **2**, 55-58.
- PUGA, E. (1990): The Betic Ophiolitic Association (southeastern Spain). *Ophioliti* **15**, 97-117.
- \_\_\_\_\_, DÍAZ DE FEDERICO, A., BARGOSI, G.M. & MORTEN, L. (1989a): The Nevado-Filábride metaophiolitic association in the Cóbdar region (Betic Cordillera, SE Spain): preservation of pillow structures and development of coronitic eclogites. *Geodin. Acta* **3**, 17-36.
- \_\_\_\_\_, \_\_\_\_\_, BODINIER, J.L., MONIÉ, P. & MORTEN, L. (1991): The Betic ophiolitic eclogites (Nevado-Filábride Complex, SE Spain). *Second Eclogite Field Symp., Terra Nova Abstr.*, 9-10.
- \_\_\_\_\_, \_\_\_\_\_ & DEMANT, A. (1995): The eclogitized pillows of the Betic Ophiolitic Association: relics of the Tethys ocean floor incorporated in the alpine chain after subduction. *Terra Nova* **7**, 31-43.
- \_\_\_\_\_, \_\_\_\_\_, FEDIUKOVA, E., BONDI, M. & MORTEN, L. (1989b): Petrology, geochemistry and metamorphic evolution of the ophiolitic eclogites and related rocks from the Sierra Nevada (Betic Cordilleras, southeastern Spain). *Schweiz. Mineral. Petrogr. Mitt.* **69**, 435-455.
- \_\_\_\_\_, NIETO J.M., DÍAZ DE FEDERICO, A., BODINIER, J.L. & MORTEN, L. (1999): Petrology and metamorphic evolution of ultramafic rocks and dolerite dykes of the Betic Ophiolitic Association (Mulhacén Complex, SE Spain): evidence of eo-Alpine subduction following an ocean-floor metasomatic process. *Lithos* **49**, 107-140.
- PUTNIS, A. (1979): Electron petrography of high-temperature oxidation in olivine from Rhum layered intrusion. *Mineral. Mag.* **43**, 293-296.
- ROSS, M., PAPIKE, J.J. & WEIBLEN, P.W. (1968): Exsolution in clin amphiboles. *Science* **159**, 1099-1102.
- ROSS, M., PAPIKE, J.J. & SHAW, K.W. (1969): Exsolution textures in amphiboles as indicators of subsolidus thermal histories. *Mineral. Soc. Am., Spec. Pap.* **2**, 275-299.
- ROSSI, G., SMITH, D.C., UNGARETTI, L. & DOMENEGHETTI, M.C. (1983): Crystal chemistry and cation ordering in the system diopside-jadeite: a detailed study by crystal structure refinement. *Contrib. Mineral. Petrol.* **83**, 247-258.
- RUIZ CRUZ, M.D., PUGA, E. & NIETO, J.M. (1999): Silicate and ore exsolutions in pseudo-spinifex olivine of the metalultramafic rocks from the Betic Ophiolitic Association: a TEM study. *Am. Mineral.* **84**, 1915-1924.
- SMITH, D.C. (1988): A review of the peculiar mineralogy of the "Norwegian coesite-eclogite Province", with crystal-chemical, petrological, geochemical and geodynamical notes and an extensive bibliography. In *Eclogite and Eclogite-Facies Rocks* (D.C. Smith, ed.). Elsevier, Amsterdam, The Netherlands (1-206).
- TENDERO, J.A., MARTÍN-ALGARRA, A., PUGA, E. & DÍAZ DE FEDERICO, A. (1993): Lithostratigraphie des métasédiments de l'association ophiolitique Nevado-Filábride (SE Espagne) et mise en évidence d'objets ankéritiques évoquant des foraminifères planctoniques du Crétacé; conséquences paléogéographiques. *C.R. Acad. Sci. Paris* **316**, Sér. II, 1115-1122.
- WOENS DREGT, C.F. & HARTMAN, P. (1969): Regular intergrowth of cummingtonite and hornblende, both with space group P2<sub>1</sub>/m. *Neues Jahrb. Mineral., Monatsh.*, 558-563.
- XU, HUIFANG, VELEN, D.R., LUO, GUFENG & JIYUE, XUE (1996): Transmission electron microscopy study of the thermal decomposition of tremolite into clinopyroxene. *Am. Mineral.* **81**, 1126-1132.

Received December 26, 1998, revised manuscript accepted August 10, 1999.